EPTT 2024
Escola de Primavera de Transição e Turbulência

ABCM
Associação Brasileira de Engenharia e Ciências Mecânicas

Analysis of vorticity transport in separated flows over wind turbine airfoils using Detached-Eddy Simulations

Gabriel Rodrigues Pinto
São Paulo State University (UNESP), School of Engineering and Sciences, Guaratinguetá
gabriel.r.pinto@unesp.br
Luiz A. C. A. Schiavo
Northumbria University, UK.
luiz.schiavo@northumbria.ac.uk
Daniel Souza Sampaio
São Paulo State University (UNESP), School of Engineering, São João da Boa Vista
daniel.s.souza@unesp.br

Abstract. *The dynamics of the structures on the separated flow over a wind-turbine airfoil is investigated through detached-eddy simulations. Two simulations considering periodicity in the spanwise direction were carried out, one with a spanwise extent equal to 30% of the chord and one with an extent of 60% of the chord. The open-source platform OpenFOAM was used to run the simulations at a Reynolds number, based on the chord, equal to 10^5. The purpose is to validate a set of data to investigate the transport of spanwise vorticity in the region of separated flow, since the balance of this quantity is of fundamental importance for the effect of rotation on the aerodynamic of horizontal-axis wind turbines' blade sections. The comparison between the two simulations show a good convergence of the time-averaged aerodynamic force with the domain width but significantly stronger fluctuations for the case with narrower domain. We will further use the data to investigate the contribution of each transport mechanism to the balance of spanwise vorticity.*

Keywords: *HAWT, separated flow, finite volume method, detached-eddy simulation*

1. INTRODUCTION

In horizontal axis wind turbines (HAWTs), blades operate at high angles of attack, particularly near the root regions. Under these conditions, boundary layer separation occurs, where the flow detaches from the blade profile surface. This separation can result in significant energy losses, increased dynamic loads on the turbine structure, ultimately compromising its lifespan and elevating operational costs. Thorough investigations into boundary-layer separation in HAWTs may contribute to the advancement of optimized blade designs, ensuring enhanced energy efficiency, structural resilience, and operational reliability.

In wind turbine dynamics, large-scale structures such as vortices and turbulent eddies, play a predominant role in modulating aerodynamic flow, directly impacting blade performance and stability (Manwell *et al.*, 2009). The rotation of the blades induces complex vortex dynamics, altering pressure distribution, boundary layer formation, and generating structural vibrations (Tian *et al.*, 2015). These structures increase turbulence intensity, disrupting the boundary layer and critically affecting the aerodynamic lift and efficiency. Numerical simulations facilitate the analysis of large-scale structure dynamics, providing valuable insights for optimized turbine blade design.

The effects of rotation add an additional layer of complexity to flow dynamics, particularly evident when wind turbine blades operate at high angles of attack, potentially leading to separated flow phenomena. Blade rotation induces a radial velocity that significantly influences the profile of the boundary layer and the pressure distribution along the blade surface. Several mechanisms of rotational effects on the boundary layer have been identified, including the delay in boundary-layer separation. This delay can be attributed to the addition of longitudinal momentum by the Coriolis force acting on fluid elements flowing transversely due to the centrifugal force (Du and Selig, 2000). Numerical simulations have shown an increase in the resistance of the boundary layer to separation in rotating wings compared to static airfoils, resulting in increased lift (Narramore and Vermeland, 1992; Hu *et al.*, 2006). Additionally, Gross *et al.* (2012) observe that centrifugal acceleration induces a radial velocity component in the boundary layer, akin to that found in swept wings, which may lead to flow instabilities, predisposing boundary-layer transition and increasing its resistance to separation.

High rotation can lead to a stationary vortex on the blade's upper surface. Pressure fluctuations on this surface, particularly in areas with significant increases due to rotation, suggest the possibility of flow separation and recirculation,

indicating a persistent vortex structure Schreck and Robinson (2003). Simulations suggest the emergence of this structure is linked to the radial component of the Coriolis force Mauro *et al.* (2017).

Corten (2001) and Lindenburg (2003) highlighted the concept of vorticity transport from the blade root to the tip driven by centrifugal force as a potential mechanism for stabilizing the leading-edge vortex observed in insect wings (Jardin and David, 2014). However, Wojcik and Buchholtz (2014) demonstrated through a vorticity balance analysis that this mechanism is insufficient to fully explain the stability of the aforementioned vortex.

This study aims to bridge this gap in knowledge by incorporating advanced vorticity transport models into DES simulations for a more comprehensive analysis of flow dynamics over the NREL S809 airfoil. This approach will allow us to investigate the behavior of large-scale flow structures and how vorticity is transported within the separated flow region. Ultimately, these insights will empower the development of more efficient, quieter, and structurally sound wind turbine designs.

2. METHODOLOGY

The selection of an appropriate airfoil is crucial in the design of horizontal axis wind turbine (HAWT) blades. The airfoil must exhibit characteristics that ensure high lift, low aerodynamic drag, and stability under various operating conditions. In this study, the airfoil chosen for this simulation is the S809 (Fig. 1), developed by the National Renewable Energy Laboratory (NREL), for computational simulations of the flow around HAWT blades.

The S809 airfoil stands out for several advantageous characteristics for wind turbine applications, as evidenced by Somers (1997). It generates high lift, tolerates surface imperfections and roughness well, exhibits low aerodynamic drag, and demonstrates a gradual and controllable stall behavior, minimizing the risks of instability. Its design results in lower negative pitching moment coefficients compared to the NACA 4421 airfoil and even more negative coefficients than the NACA 23021 airfoil, both widely used in horizontal axis wind turbine (HAWT) blades (Somers, 1997).

The development of this project is based on numerical simulations conducted using the OpenFOAM software, an open-source platform dedicated to computational fluid dynamics (CFD) simulation. CFD plays a significant role in modeling and analyzing fluid behavior. Among the various CFD techniques, the Detached Eddy Simulation (DES) hybrid approach stands out for its precision and efficiency (Spalart *et al.*, 2006) .

Based on dividing the flow into two distinct regions, DES combines the accuracy of Large Eddy Simulation (LES) with the computational efficiency of Reynolds-Averaged Navier-Stokes (RANS) turbulence modeling. In areas near walls and in high-turbulence zones, where precision is crucial, DES utilizes LES's ability to represent large turbulent eddies with fidelity. On the other hand, in regions farther from walls and with lower turbulence, DES employs RANS, taking advantage of its computational efficiency. This synergy between LES and RANS allows DES to be widely used in flow analysis, providing remarkable accuracy at an optimized computational cost.

The DES simulations in this project were performed using the PIMPLE solver in OpenFOAM. The PIMPLE (Pressure-Implicit, Momentum-Implicit, Coupled-Explicit) is a multiphase solver that stands out for its ability to handle complex problems involving multiphase flows and moving interfaces. To model turbulence in the flow around the airfoil, the k-ω SST (Shear Stress Transport) (Menter, 1994) model was employed, recognized for its effectiveness in capturing a wide range of turbulent phenomena, from separation and recirculation regions to turbulent boundary layers, proving particularly useful in complex flows. This model combines the advantages of the k-ω model (Wilcox, 1988) in regions near walls and the k-ε model (Launder and Spalding, 1974) in regions away from walls, favoring accurate simulation of turbulent effects in different parts of the flow.

In this study, a periodicity condition was considered in the spanwise direction, performing two simulations with different widths: one with 0.3 of the chord and another with 0.6 of the chord, aiming to evaluate the sensitivity of the model. Figure 1 illustrates the approach adopted in the mesh, which follows the C-type mesh pattern, with refinement in the boundary layer and wake regions. The mesh structure is composed of a total of 1,908,900 elements, covering a simulation domain with dimensions of 50c (chords) in both directions. The growth rate of the volumes in the direction perpendicular to the airfoil surface is 1.1. The maximum value of y^+ in the elements adjacent to the airfoil surface is approximately 1.3. At the outer boundary of the computational domain, fixed values were imposed for the velocity and zero pressure gradient for regions of inflow and fixed pressure and zero velocity gradient conditions were applied gradient for regions of outflow, while for the airfoil, the no-slip wall condition applied. Furthermore, it's important to highlight that an incompressible flow is assumed due to the low Mach number near the root. The angle of attack is 16°, and the Reynolds number employed is 10^5, to minimize computational cost.

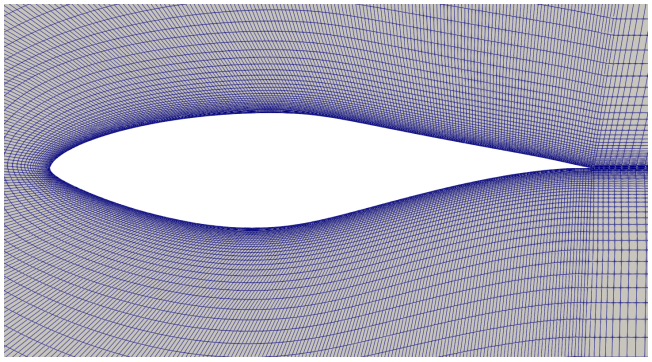

Figure 1. Mesh detail near the airfoil.

3. RESULTS AND DISCUSSIONS

To identify and exclude the initial transient state, the flow simulations for the S809 airfoil profile at domains size of 0.3 and 0.6 in z (L_z) we initially analyzed. The analysis focuses on a time interval within the total simulation of 45 convective times, $\tilde{t} = tU_\infty/c$, where t is the time, U_∞ is the freestream velocity and c is the airfoil chord. For the domain of 0.3, $\tilde{t}$ between 30 and 75 were chosen, while for the domain of 0.6, the focus is on $\tilde{t}$ between 15 and 60. Figure 2 shows the streamlines and z vorticity contours for the a time averaged flow in the Z direction (L_z= 0.3 and L_z = 0.6, respectively) over an airfoil. Through the analysis of these figures, it is possible to gain an understanding of the flow behavior and identify key features that influence the aerodynamics of the airfoil. The streamlines reveal a separated flow pattern on the entire airfoil's upper surface. Upon examining the vorticity distribution at the leading edge, a boundary layer detachment is identified.

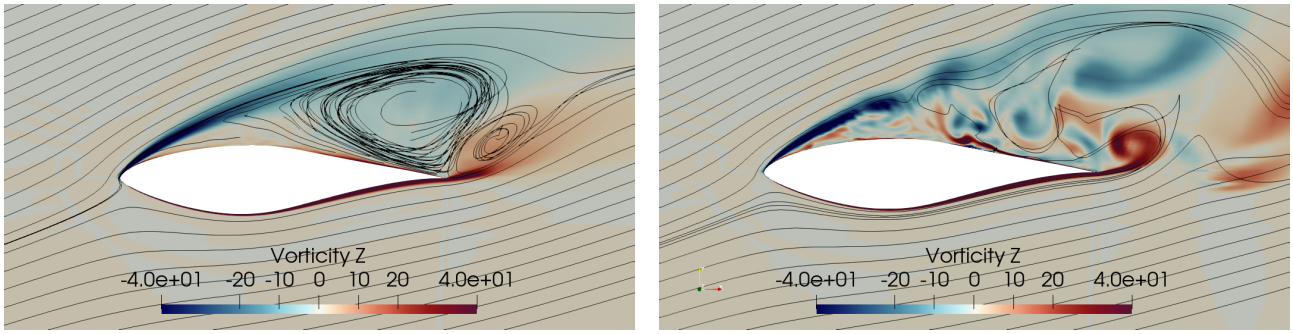

Figure 2. Mean spanwise-components-vorticity field along with streamlines for (a) L_z= 0.3 and (b)L_z= 0.6.

Figure 3 compares the average pressure coefficient distribution over the airfoil center span for L_z = 0.3 and L_z = 0.6, normalized by the chord length. The pressure distribution graph shows a sharper suction peak for the L_z = 0.3, indicating a higher lift force at this location. The almost uniform pressure across the upper surface for both L_z values (0.3 and 0.6) expected due to the presence of boundary layer separation, evidenced in figure 2.

In figures 4a and 4b, the graphs of the coefficients C_l and C_d are presented. The analysis of these figures aims to understand the underlying reasons for the fluctuations in the values of these coefficients. In figure 4a, it is noticeable that there are more intense peaks and local minimum for larger and smaller values of C_l for L_z = 0.3 and the observation is the same for C_d values, with more pronounced peaks and local minimum for the domain size L_z=0.3.

For L_z = 0.3, the highest value of C_l is 1.1729 and the lowest is 0.3648, while for L_z = 0.6, the highest value of C_l is 0.9787 (15.54% less) and the lowest is 0.4535 (24.31% more). Regarding the value of C_d, for L_z = 0.3, a greater than 0.43 is obtained and the lowest is around 0.22. For the L_z = 0.6 domain, the highest value is approximately 0.34 and the lowest is also around 0.22.

The table 1 shows the mean and standard deviation of C_l and C_d. As predicted in the discussions of fig. 4, L_z= 0.3 had the highest mean C_l, but also the highest average drag C_d with percentage error obtained between the averages was 6% for C_l and 3.5% for C_d. The intense fluctuations, observed in figure 4 for L_z= 0.3, justify the higher standard deviation of the coefficients.

The peaks and local minimum of each domain in z (L_z = 0.3 and L_z = 0.6) in Fig. 4 underwent a detailed analysis using the Q Criterion, which allows the identification of vortex cores, being useful for understanding the dynamics of large-scale structures in the flow. Figures 5a, 6a, 7a, and 8a depict the instantaneous field of the spanwise vorticity component in the central section of the domain, iso-surfaces of the Q criterion, and the pressure distribution on the airfoil's upper surface.

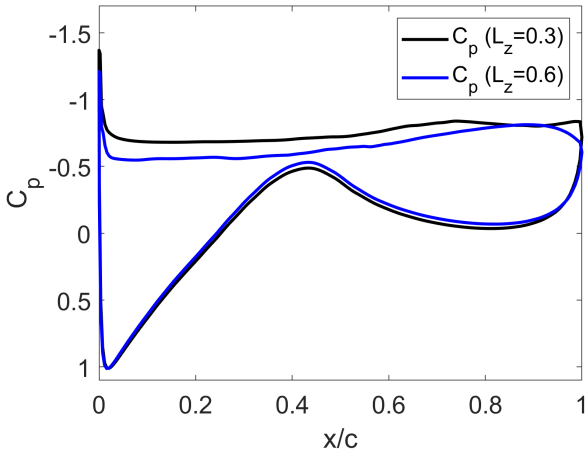

Figure 3. Mean pressure coefficient distribution(C_p) over the airfoil center span

.

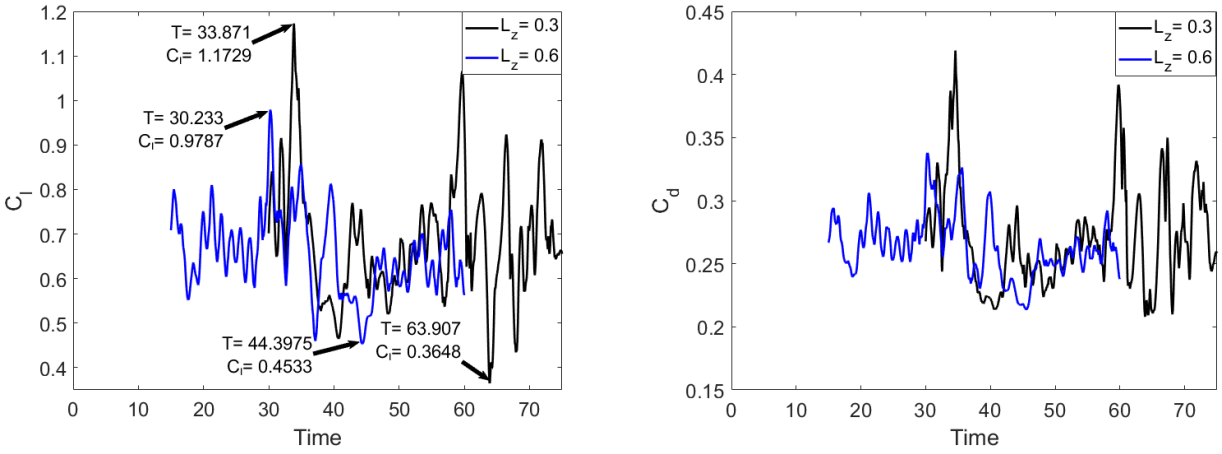

(a) (b)

Figure 4. Time evolution of (a) lift coefficient (C_l) and (b) drag coefficient (C_d).

Table 1. Coefficientes C_l e C_d for the domains Lz=0.3 and Lz=0.6.

Lz	Mean C_l	Std. dev. of C_l	Mean C_d	Std. dev. (C_d)
0.3	0.682105	0.148210	0.269489	0.045162
0.6	0.643515	0.095127	0.260263	0.025720

Figures 5b, 6b, 7b, and 8b illustrate the instantaneous C_p distribution on the central section of the airfoil.

Figures 5a and 6a reveal the presence of a mixing layer at the airfoil's leading edge. The observation of substantial vortex cores within the mixing layer suggests the possible occurrence of Kelvin-Helmholtz instability. Near the airfoil's trailing edge, a significant concentration of vortex cores is observed. This concentration leads to a local reduction in pressure, as evidenced by figures 5b and 6b between x/c = 0.60 and 0.85 approximately. This reduction in pressure may be related to the observed increase in C_l (fig. 5a), additionally, the pressure reduction may contribute to the increase in C_d (as presented in fig. 4b). In the wake of the airfoil, the presence of longitudinal vortices between the primary vortices is identified, contributing to the flow complexity.

In the local minimum regions, represented by figures 7a and 8a, a less prominent mixing layer is observed compared to the previous images (figures 5a and 6a). This mixing layer extends with less intensity, although vortex cores are still observed. A well-organized positive vortex near the trailing edge can be identified in both figures 7a and 8a, which may explain the sharp reduction in C_p at the trailing edge for theL_z= 0.3 case and a slight reduction in C_p at the trailing edge for the L_z= 0.6 case, as shown in figures 7b and 8b. The absence of significant vortex cores results in a relatively low value of C_l (Fig. 4a) and a higher value of pressure on the upper surface.

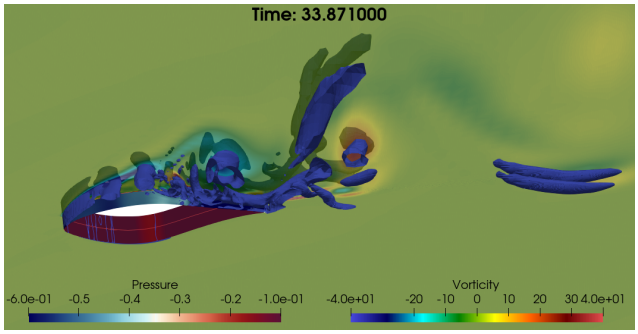

(a)

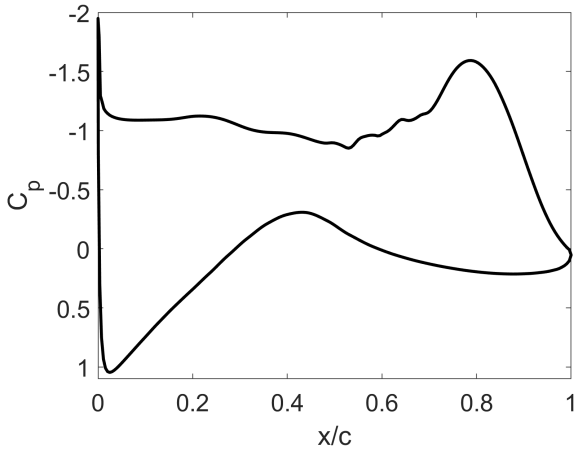

(b)

Figure 5. (a) Instantaneous flow field (spanwise vorticity Q-criterion and surface pressure) and (b) C_p at a C_l-peak time for L_z= 0.3.

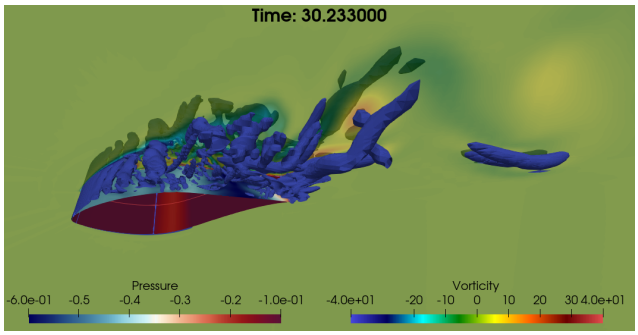

(a)

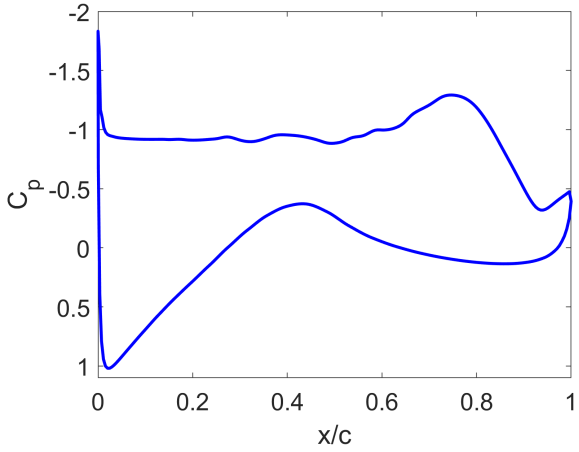

(b)

Figure 6. (a) Instantaneous flow field (spanwise vorticity Q-criterion and surface pressure) and (b) C_p at a C_l-peak time for L_z= 0.6.

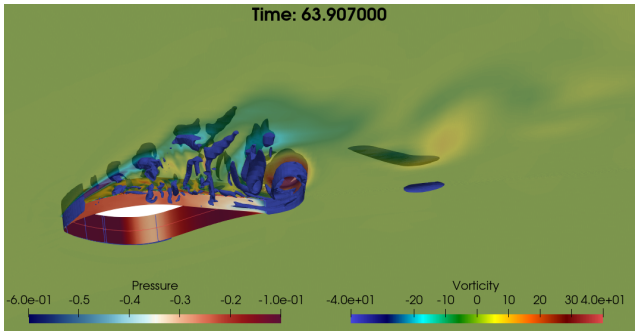

(a)

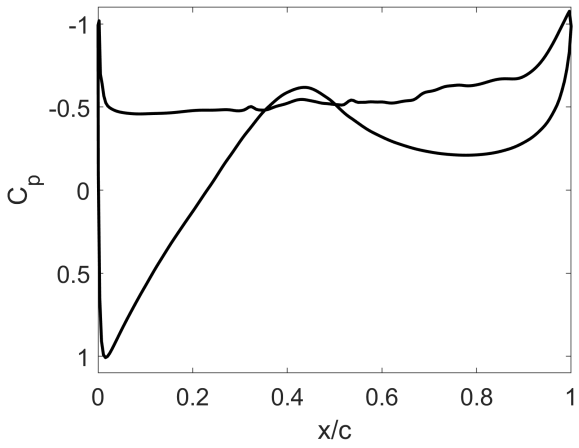

(b)

Figure 7. (a) Instantaneous flow field and (spanwise vorticity Q-criterion and surface pressure) (b) C_p at a local minimum of C_l for L_z= 0.3.

Figures 5 and 6 provide a possible explanation for the discrepancy in force fluctuations between $L_z = 0.3$ and

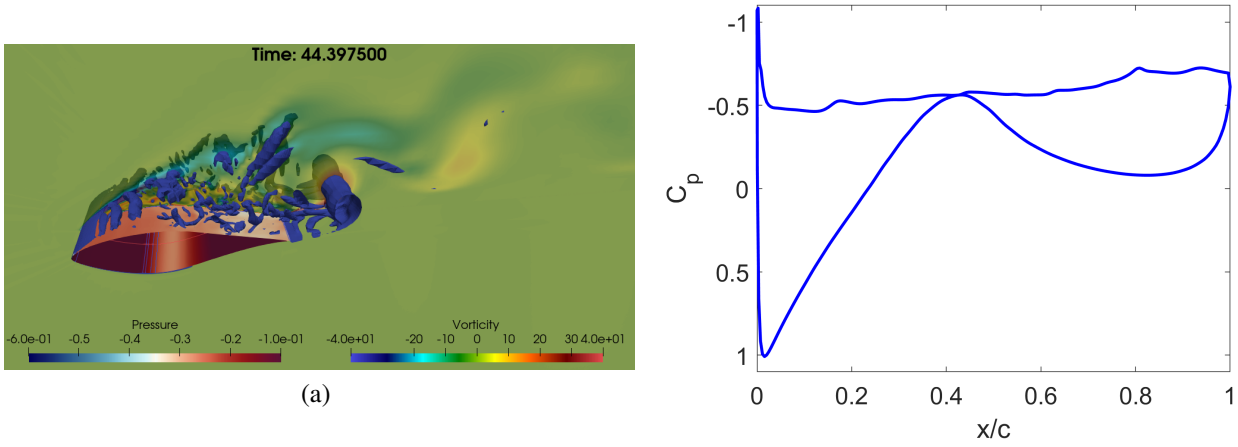

(a) (b)

Figure 8. (a) Instantaneous flow field (spanwise vorticity Q-criterion and surface pressure) and (b) C_p at a local minimum of C_l for L_z= 0.6.

$L_z = 0.6$ (Fig. 4). A greater organization of structures is observed in the $L_z = 0.3$ case, likely due to its configuration being closer to 2D. This can be attributed to the capability of the $L_z = 0.6$ simulation to capture some three-dimensional structures that are not observed in $L_z = 0.3$. These additional structures may interfere with the organization of Kelvin-Helmholtz vortices, which are predominantly 2D, resulting in a reduction in the amplitude of force fluctuations.

To analyze vorticity transport, the time-averaged convective, stretching, and diffusive terms were integrates along a region encompassing the recirculating flow for the case with Lz=0.3. Figure 9 shows region of integration.

The convective term exhibited the highest value, 0.9003, followed by the stretching term, -0.1539, and the diffusive term, -0.0921, indicating that convection is the dominant mechanism for vorticity transport.

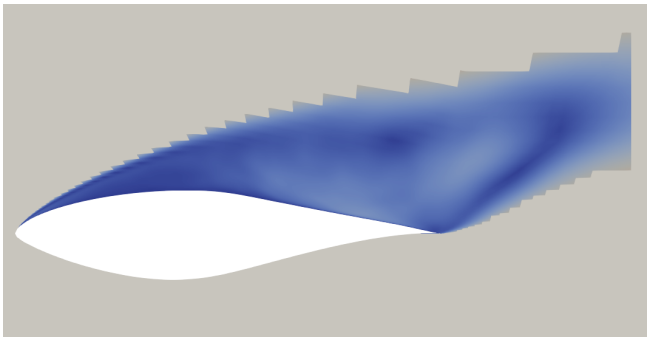

Figure 9. Region considered for the analysis of vorticity transport terms

4. CONCLUSIONS

Simulations were performed with varying spanwise dimensions. Comparisons of time-averaged results show three-dimensional effects in simulation Lz=0.6, not observed in Lz=0.3. This highlights the importance of a longer spanwise for developing 3D instabilities in this range of Reynolds number. The simulations captured flow characteristics typical of high angles of attack, including leading-edge separation. Comparison between simulations with different spanwise domain extension showed good convergence of the time-average quantities. However, the simulations with wider computational domain predicted weaker fluctuations of the aerodynamic forces. This difference is probably due to a reduction of the Kelvin-Helmholtz-vortex coherence. For the L_z= 0.3 case, an in-depth analysis of vorticity transport within the separated flow region has been conducted, including the calculation of the vorticity balance.

5. ACKNOWLEDGEMENTS

This study was financed in part by the Coordenação de Aperfeiçoamento de Pessoal de Nível Superior - Brasil (CAPES) - Finance Code 001. This research was supported by resources supplied by the Center for Scientific Computing (NCC/GridUNESP) of the São Paulo State University (UNESP). The authors also acknowledge support from Conselho Nacional de Desenvolvimento Científico e Tecnológico (CNPq)(Processo: 423369/2021-0).

6. REFERENCES

Corten, G., 2001. *Flow separation on wind turbine blades*. Ultrecht, Netherlands.

Du, Z. and Selig, M., 2000. "The effect of rotation on the boundary layer of a wind turbine". *Renewable Energy*, Vol. 20, pp. 167–181.

Gross, A., Fasel, H., Friderich, T. and Kloker, M., 2012. "Numerical investigation of rotational augmentation for s822 wind turbine airfoil". *Wind Energy*, Vol. 15, pp. 987–1007.

Hu, D., Hua, O. and Du, Z., 2006. "A study on stall-delay for horizontal axis wind turbine". *Renewable Energy*, Vol. 31, pp. 821–836.

Jardin, T. and David, L., 2014. "Spanwise gradients in flow speed help stabilize leading-edge vortices on revolving wings". *Physical Review E*, Vol. 90, No. 1, pp. 312–340.

Launder, B.E. and Spalding, D.B., 1974. "The numerical computation of turbulent flows". *Computer methods in applied mechanics and engineering*, Vol. 3, pp. 269–289.

Lindenburg, C., 2003. "Investigation into rotor blade aerodynamics". Technical report, NOVEM.

Manwell, J.F., McGowan, J.G. and Rogers, A.L., 2009. *Wind energy explained: Theory, design, and application*. John Wiley & Sons.

Mauro, S., Lanzafame, R. and Messina, M., 2017. "An insight into the rotational augmentation on hawts by means of cfd simulations - part ii: Post processing and force analysis". *International Journal of Applied Engineering Research*, Vol. 12, No. 21, pp. 10505–10529.

Menter, F.R., 1994. "Two-equation eddy-viscosity turbulence models for engineering applications". *AIAA journal*, Vol. 32, No. 8, pp. 1598–1605.

Narramore, J. and Vermeland, R., 1992. "Navier-stokes calculations of inboard stall delay due to rotation". *Journal of Aircraft*, Vol. 29, No. 1, pp. 73–78.

Schreck, S. and Robinson, M., 2003. "Boundary layer state and flow field structure underlying rotational augmentation of blade aerodynamic response". *Transactions of the ASME*, Vol. 125, pp. 448–456.

Somers, D.M., 1997. "Design and experimental results for the S809 airfoil". *National Renewable Energy Laboratory (NREL)*.

Spalart, P., Deck, S., Shur, M., Squires, K.D., Strelts, M.K. and Travin, A., 2006. "A new version of detached-eddy simulation, resistant to ambiguous grid densities". *Theoretical and Computational Fluid Dynamics*, Vol. 20, pp. 181–195.

Tian, W.M., Zhao, Y., Lin, X. and Liu, Y., 2015. "Effects of blade rotation on vortex shedding from a bluff body". *Journal of Fluids and Structures*, Vol. 54, pp. 123–138.

Wilcox, D.C., 1988. "Re-assessment of the 2-equation k- turbulence model". *AIAA journal*, Vol. 26, No. 2, pp. 219–226.

Wojcik, C. and Buchholtz, J., 2014. "Vorticity transport in the leading-edge vortex on a rotating blade". *Journal of Fluid Mechanics*, Vol. 743, pp. 249–261.

7. RESPONSIBILITY NOTICE

The authors are the only responsible for the printed material included in this paper.